# Numerical Analysis for Lateral Grain Growth of Poly-Si Thin Films Controlled by Laser-Induced Periodic Thermal Distribution

Hirokazu Kaki, Yasunori Nakata and Susumu Horita
JAIST (Japan Advanced Institute of Science and Technology), Tatsunokuchi, Ishikawa 923-1292, Japan

## ABSTRACT

In order to obtain a large Si grain and to control the location of grain boundary in a Si film thermally melting-crystallized by pulse laser, we have proposed to use a periodic thermal distribution spontaneously induced by a linearly polarized laser beam. The lateral grain growth of polycrystalline Si thin films, which is controlled by the laser-induced periodic thermal distribution, was analyzed numerically by two-dimensional finite element computer simulations. From this analysis, it can be conclude that the laser irradiation should be performed to melt not all but most of Si film or melt it partially, making the large difference between the maximal and minimal temperature in the thermal distribution. It was also found that the temperature difference was increased with the optical absorption in the Si film and the fluence.

## INTRODUCTION

Recently, amorphous silicon (a-Si) thin film transistors (TFT's) are widely utilized in the active matrix liquid crystal displays (LCD's). In the near future, larger size and higher resolution LCD's are required not only as monitors of personal computers but also as high-resolution LCD-TV's. In order to produce such LCD's, higher performance TFT's and system-on-glass technology are required. So, polycrystalline silicon (poly-Si) films attract much attention because the mobility of poly-Si is 1 or 2 orders larger than a-Si.

The pulse laser annealing (PLA) method is effective to produce the poly-Si film of larger grain with the high carrier mobility on a glass substrate [1,2]. In order to obtain a larger grain and to control the location of grain boundary, it is necessary to make the temperature distribution in the molten Si film to be suitable for grain growth. Then, we proposed to use the periodic thermal distribution spontaneously induced by a linearly polarized laser beam [3]. For most of the case, this periodic spacing $\Lambda$ is formulated by Rayleigh's diffraction conditions as

$$\Lambda \approx \frac{\lambda}{n_0\left(1 \pm \sin\theta_i\right)} \tag{1}$$

for a *p*-polarized beam, where $\lambda$ is the incident laser wavelength, $\theta_i$ is the angle from the normal incidence and $n_0$ is the refractive index of the incident medium above the surface. In fact,

by using a linearly polarized laser beam, we obtained a Si grain as large as the wavelength of the laser beam on a pyrex glass substrate and aligned the grain boundaries in parallel with one another.

In this paper, by using numerical analysis, we calculated the temperature distribution induced by the sinusoidal periodic heating source and investigated the lateral grain growth of poly-Si film from the molten Si. The crystallization process was analyzed by two-dimensional finite element computer simulations of the heat transport and the phase transitions during laser melting-crystallization.

## SIMULATION MODEL

Our crystallization method induces a temperature distribution in both the direction perpendicular to the film (z direction) and the direction along the plane of incidence of the laser beams (x direction). Thus, a 2-dimensional simulation of the crystallization process is necessary. According to the model developed by Wood *et al.* [4], the 2-dimensional finite difference heat transport equation is given by

$$\rho\frac{h_{i,j}^{(t+1)}-h_{i,j}^{(t)}}{\Delta t}=\frac{1}{(\Delta x)^2}\left(\frac{K_{i+1,j}+K_{i,j}}{2}\left(T_{i+1,j}^{(t)}-T_{i,j}^{(t)}\right)+\frac{K_{i,j}+K_{i-1,j}}{2}\left(T_{i-1,j}^{(t)}-T_{i,j}^{(t)}\right)\right)$$
$$+\frac{1}{(\Delta z)^2}\left(\frac{K_{i,j+1}+K_{i,j}}{2}\left(T_{i,j+1}^{(t)}-T_{i,j}^{(t)}\right)+\frac{K_{i,j}+K_{i,j-1}}{2}\left(T_{i,j-1}^{(t)}-T_{i,j}^{(t)}\right)\right)+S_{i,j}^{(t)}. \quad (2)$$

Here, $h_{i,j}^{(t)}$ is the enthalpy of $(i, j)$ cell at the time $t$, $\rho$ is the density of the material, $K_{i,j}$ is the temperature dependent thermal conductivity, $T_{i,j}^{(t)}$ is the temperature, and $S_{i,j}^{(t)}$ is the heat source term that includes the absorption of the incident laser radiation. It has been reported that the induced periodic temperature distribution is originated from the interaction among the incident beam, the diffracted beam and the random surface roughness, and the positive feed back system enhances the periodic temperature and the periodic surface roughness. The detailed mechanism is discussed elsewhere [5]. We assumed that the periodic temperature distribution is induced by the spatial laser profile intensity $P_n$,

$$P_n \cong P_0\left[1+P_1\cos\left(\frac{2\pi}{\Lambda}x+\phi_p\right)\right], \quad (3)$$

based on the model of Guosheng *et al.* [6]. Here, $P_0$ is the average laser intensity, $\phi_p$ is the amplitude of the sinusoidal laser profile intensity, and $P_0P_1$ is the phase difference between sinusoidal surface roughness and laser profile intensity. Although the surface roughness is important to produce $P_n$, we assumed that the irradiated surface is flat without roughness for simplifying the calculation.

Basically, at every time step $\Delta t$, the model calculates the temperature distribution of all cells, taking the contribution of the laser pulse into account. It then keeps track of the phase

changes and the release of latent heat in each cell by considering its temperature and comparing it with its neighbors using the state array matrix (see Ref. 4). This matrix contains the information of the phase diagram of the a-Si/crystal-Si(c-Si)/poly-Si/liquid-Si system and one timer. The timer, $t_n$, is used to simulate nucleation events. It is defined as the incubation time required for the appearance of nucleation sites in the supercooled liquid-Si and corresponds to the inverse of the bulk nucleation rate. A necessary condition for nucleation is that the cell under consideration must contain supercooled liquid-Si at a temperature lower than the so-called nucleation temperature $T_n$.

The material parameters are summarized in Table I. The time step $\Delta t$ is $1\times10^{-13}$ s, which is smaller than the stability criterion for this system using finite elements with dimensions $\Delta x$ =10 nm and $\Delta z$ =5 or 10 nm. The typical simulation conditions are as follows; The nucleation timer $t_n$ =8 ns, the nucleation temperature $T_n$ =1523.15 K, the initial film state is poly-Si, the pulse width of incidence laser is 6.5 ns and the incident angle $\theta_i = 0$. In case of normal incidence, $\phi_p$ is 0 according to Guosheng's model [6]. In Eq. (3), $P_0P_1$ is equivalent to the sinusoidal surface roughness of 3 nm and $\Lambda$ is a spatial period of 530 nm corresponding to the Nd:YAG laser wavelength of 532 nm in the experiment.

## RESULTS AND DISCUSSION

Figure 1 shows the film thickness dependences on the temperature difference $T_d$ at the fluence of 100 and 150 mJ/cm$^2$, where the substrate temperature is 500 K and $\Delta z$ = 5 nm. $T_d$

**Table I**. Material parameters used in the simulations. $\alpha$, $n$, $k$, $L$, $T_m$, $\rho$, $c_p$ and $K$ denote the absorption coefficient, the refractive coefficient, the attenuation coefficient, the latent heat, the phase change temperature, the density, the specific heat and the thermal conductivity, respectively. Further details of the functional dependences and of the parameter values are found in the Refs. 7 and 8.

| Parameters | poly-Si | fine-Si | a-Si | liquid-Si |
|---|---|---|---|---|
| $\alpha$ [cm$^{-1}$] | 9380exp(T/430) | ------ | ------ | 1.13x10$^6$ |
| $n$ | 4.153+5x10$^{-5}$(T+273.15) | ------ | ------ | 2.35 |
| $k$ | 0.0397exp(T/430) | ------ | ------ | 4.8 |
| $L$ [J/g] | 1800 | | 1320 | ------ |
| $T_m$ [K] | 1683.15 | | 1423.15 | ------ |
| $\rho$ [g/cm$^3$] | 2.33 | | | |
| $c_p$ [J/g K] | 0.7+sqrt((T-300)/15556) | | | 1 |
| $K$ [J/s cm K] | 0.75exp(-(T-300)/764) | 0.05 | 0.01 | 0.25+9.4x10$^{-5}$(T-1700) |

indicates the difference between maximal and minimal temperatures or twice amplitude in the periodic temperature distribution generated by $P_n$. From this figure, it is found that $T_d$ has maxima every 60 nm and their values decrease with the film thickness. This phenomenon can be explained as follows; From the calculation of the optical absorptivity of a poly-Si film on an $SiO_2$ substrate considering multiple reflections, the absorptivity has maxima every 60 nm. However, increasing the film thickness increases lateral thermal conduction of the molten Si film and reduces the temperature difference in the periodic temperature distribution. From this result, it can be said that the suitable thickness is about 60 nm for our method. Further, from Fig. 1, $T_d$ at the fluence of 150 mJ/cm$^2$ is higher than 100 mJ/cm$^2$. The detail of this tendency is shown in Fig. 2, where the substrate temperature is 500 K, the thickness of Si film is 60 nm and $\Delta z$ =10 nm. From this result, it can be seen that the temperature difference increases with the fluence. Therefore, from the calculation result, it seems that the increasing fluence is more suitable to control the grain boundary location since the lateral growth of crystallized Si from minimal to maximal temperature points is more enhanced by larger temperature difference.

Figures 3 and 4 show the simulation results of crystallization process at 140 and 180 mJ/cm$^2$, respectively, in time sequence after shot of the laser pulse, where $\Delta z$ =10 nm. In these figures, the crystallization process is presented only in the one spatial period of $\Lambda$, and the positions of the maximal and minimal laser intensity are the center and both of the edges, respectively. In the case of 140 mJ/cm$^2$, most of the Si film is molten by laser irradiation but a little poly-Si is non-molten at both the points of minimal laser intensity and the interface to the substrate. This poly-Si region becomes a seed for crystallization. So, at $t$ =13 ns after laser irradiation of Fig. 3(a), the c-Si is generated at this position and the intermediate mixed-phase of liquid and crystalline Si (mixed-Si) is formed. The liquid Si cools down until nucleation occurs. The cooling rate toward the center is faster than the surface because the temperature gradient to

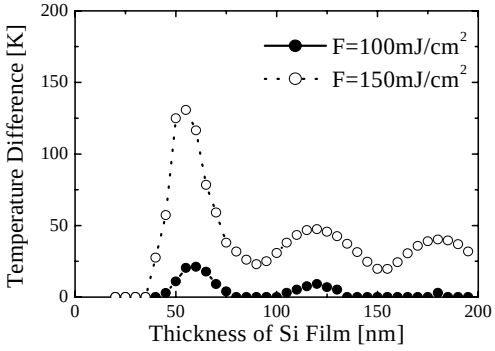


**Figure 1.** Dependence of the temperature difference on the thickness of Si film at the fluence of 100 (closed circle) and 150 mJ/cm$^2$ (open circle), respectively. The substrate temperature is 500 K.

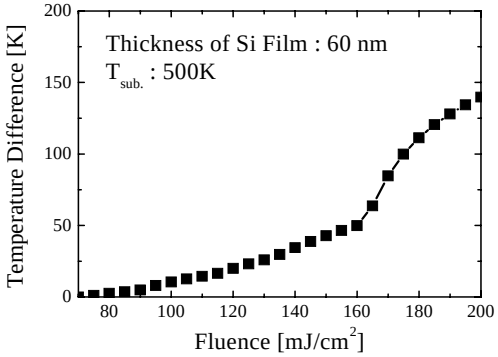


**Figure 2.** Fluence dependence of the temperature difference in the Si film with 60 nm thickness at 500 K.

the center is larger than the surface. Thus, the crystallization progresses as shown in Fig. 3(b) of $t$=100 ns. Finally, at 161 ns of Fig. 3(c), the crystallization is finished completely, and poly-Si region is formed at the center of the film surface where the grain boundary is generated. On the other hand, in case of larger fluence 180 mJ/cm$^2$, by laser irradiation, all of Si film is completely molten as shown in Fig. 4(a). This completely melting state induces the supercooled liquid-Si because crystallization without a seed does not occur within nucleation time. After the nucleation time, spontaneous nucleation occurs near the interface where the temperature is the lowest. Then, at 78 ns of Fig. 4(b), the fine crystalline Si (fine-Si) region is formed. Finally, at 240 ns of Fig. 4(c), although the crystallization progress is finished completely and a poly-Si region is formed at the center of the film surface like Fig. 4(c), this crystallized Si film contains many poly-Si and fine-Si grains near the interface. From the simulation results of Figs. 3 and 4, it can be concluded that laser irradiation should be performed to melt not all but most of Si film like Fig. 3 in order to control the grain boundary alignment in the crystallized Si film for our method. Therefore, we should adjust the fluence from viewpoints of not only the temperature difference of Fig. 2 but also the melting state of the Si film.

Figure 5 shows the fluence dependences of the melt depth at the center and the edge of the one periodic space of the irradiated sample, where the substrate temperature is 500 K, the film thickness is 60 nm and $\Delta z$=10 nm. The positions of maximal and minimal $P_n$ are the center and both the edges, respectively. We can see from this figure that the melting depths of the center and the edge are increased almost linearly with the fluence up to near 150 mJ/cm$^2$. Over 160 mJ/cm$^2$, all of the Si film is completely molten. So, it can be deduced that the suitable fluence is

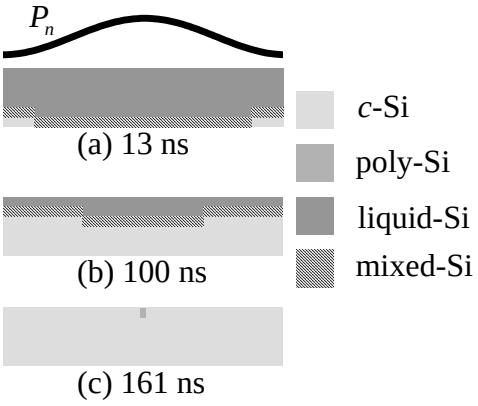


**Figure 3.** 2-dimensional simulations of crystallization process at 140 mJ/cm$^2$. The sequential times are (a)13 ns, (b)100 ns, and (c)161 ns after a shot of the laser pulse. Each diagram shows a cross section of the Si film with 60 nm thickness and 530 nm width.

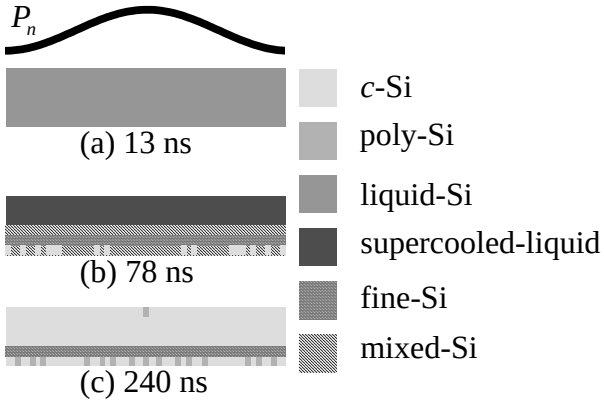


**Figure 4.** 2-dimensional simulations of crystallization process at 180 mJ/cm$^2$. The sequential times are (a)13 ns, (b)78 ns, and (c)240 ns after a shot of the laser pulse. Each diagram shows a cross section of the Si film with 60 nm thickness and 530 nm width.

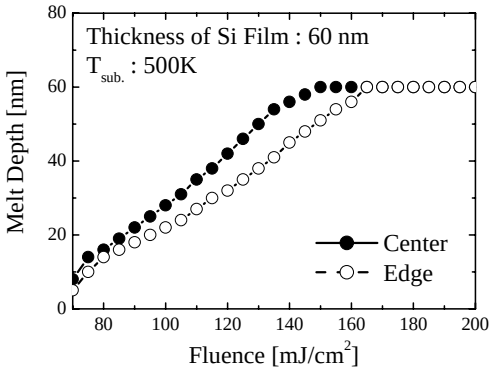


**Figure 5.** Fluence dependences of the melt depth of the Si film with 60 nm thickness at 500 K.

from 150 to 160 mJ/cm$^2$, in which the center of the film is completely molten and its edges are partially molten.

## CONCLUSIONS

We investigated the lateral grain growth of poly-Si film from molten Si whose temperature distribution is sinusoidal periodic. This analysis suggests that the suitable thickness be about 60 nm and that the laser irradiation should be performed to melt not all but most of Si film or melt it partially, making a large difference between the maximal and minimal temperature in the thermal distribution in order to control the grain boundary location for our method.

## REFERENCES

1. T. Sameshima, S. Usui, and M.Sekiya, IEEE Electron Device Lett. **7**, 276 (1986).
2. K. Sera, F. Okumura, H. Uchida, S. Itoh, S. Kaneko, and K. Hotta, IEEE Electron Device Lett. **36**, 2868 (1989).
3. S. Horita, Y. Nakata, and A. Shimoyama, Appl. Phys. Lett. **78**, 2250 (2001).
4. R. F. Wood, and G. A. Geist, Phys. Rev. B **34**, 2606 (1986).
5. Anthony E. Siegman, and Philippe M. Fauchet, IEEE J. Quantum Electron. **QE-22**, 1384 (1986).
6. Zhou Guosheng, P. M. Fauchet, and A. E. Siegman, Phys. Rev. B **26**, 5366 (1982).
7. R. F. wood, C. W. White, and R. T. Young, SEMICONDUCTORS AND SEMIMETALS **23**, ACADEMIC PRESS (1984).
8. G.. Aichmayr, D. Toet, M. Mulato, P. V. Santos, A. Spangenberg, S. Christiansen, M. Albrecht, and H. P. Strunk, J. Appl. Phys. **85**, 4010 (1999)